

Design and Analysis of 2- μm InGaSb/GaSb Quantum Well Lasers Integrated Onto Silicon-on-Insulator (SOI) Waveguide Circuits Through an Al_2O_3 Bonding Layer

Xiang Li, Hong Wang, Zhongliang Qiao, Yu Zhang, Zhichuan Niu, Cunzhu Tong, *Member, IEEE*, and Chongyang Liu, *Member, IEEE*

Abstract—GaSb-based quantum well (QW) laser diode, with emission wavelength $\sim 2\ \mu\text{m}$, integrated onto a silicon-on-insulator (SOI) waveguide circuit through a high-thermal-conductivity Al_2O_3 bonding layer has been designed and analyzed. Prior to bonding, the fabricated Fabry–Perot GaSb QW laser worked under continuous wave operation at room temperature, with a low threshold current of 37 mA at the emission wavelength of 2019 nm, demonstrating high material quality. A tapered structure has been used for evanescent coupling of light from the GaSb laser to the underlying Si waveguide. Instead of using SiO_2 for direct bonding or Benzocyclobutene for adhesive bonding, the use of Al_2O_3 to directly bond GaSb lasers onto SOI wafers is proposed. The optical mode distribution simulations by a beam propagation method software show that light can be coupled efficiently to the underlying Si waveguide through the tapered structure without compromise in optical coupling efficiency. Furthermore, there is a significant reduction ($\sim 70\%$) in the total thermal resistance compared with the same structure using a SiO_2 bonding layer. Our results suggest that the Al_2O_3 bonding layer could be a promising candidate for III–V lasers integrated on SOI circuits, where thermal dissipation is very critical.

Index Terms— Al_2O_3 wafer bonding, GaSb laser, Quantum well, silicon photonics, silicon-on-insulator (SOI), tapered structure.

I. INTRODUCTION

HIGH-performance light sources operating at 2 μm and above are key components for applications such

as gas sensing, medical diagnostics as well as advanced telecommunication [1]–[5]. Such optical emitting devices are normally based on III–V compound semiconductor materials, such as InP-based [6], [7] and GaSb-based [8], [9] quantum well (QW) laser structures. Though high performance 2- μm laser diodes have been demonstrated from both systems, GaSb-based QW lasers are less critical in material growth compared to the highly strained InGaAs QW on InP for wavelength around 2 μm . Thus it is more advantageous for wavelengths longer than 2 μm .

On the other hand, silicon photonics, based on silicon-on-insulator (SOI) waveguide circuits, is a well-established CMOS compatible technology, which enables the compact passive silicon photonic circuits [10]. However, due to the intrinsic material property, i.e., indirect bandgap, the Si-based materials cannot emit light efficiently.

If the strength of these two worlds can be combined, namely, the integration of III–V lasers onto SOI waveguide circuits, it potentially allows the highly compact gas sensing and optical communication devices to have a large degree of freedom in device design, thus improving the system performance. Furthermore, these devices can be fabricated using the mature CMOS process infrastructure, resulting in high yield, high volume production and therefore low cost [11].

There are quite a few papers addressing the integration of III–V laser structures onto SOI platforms [12]–[20]; however, most of them are based on InP-based materials at telecom wavelength of 1.55 μm . So far, there are few reports on the design of lasers, integrated onto SOI platforms, with emission wavelength around 2 μm and above. And even in these limited reports, the device performance still needs to be further improved in terms of working temperature and output power [17]. For example, Hattasan *et al.* has reported the first GaSb-based laser integrated onto a SOI waveguide, working under continuous wave (CW) operation with output power of a few tens of μW only. Furthermore, the GaSb Fabry–Perot (FP) laser was bonded onto an InP carrier first and then bonded onto the SOI platform. Though the pioneering result demonstrated the possibility of integrating a GaSb-based laser onto a SOI, this laser design limits light coupling efficiency from lasers to Si waveguides. Therefore, direct GaSb laser integrated onto a SOI platform is greatly desired. In addition, the GaSb-based material has higher refractive index (3.896 for GaSb) [21] than Si (3.451) [22]. Therefore, intrinsically, the light is not easy to couple down from the higher-index GaSb QW

Manuscript received January 28, 2016; revised April 2, 2016; accepted April 5, 2016. Date of publication April 25, 2016; date of current version June 30, 2016. This work was supported in part by the National Research Foundation of Singapore NRF-CRP12-2013-04, NTU-A*Star Silicon Technologies Centre of Excellence, and National Natural Science Foundation of China under Grant 61435012.

X. Li and Z. Qiao are with the School of Electrical and Electronic Engineering, Nanyang Technological University, Singapore 637553 (e-mail: E140151@e.ntu.edu.sg; zliqiao@ntu.edu.sg).

H. Wang is with the Temasek Laboratories as well as with the School of Electrical and Electronic Engineering, Nanyang Technological University, Singapore 637553 (e-mail: ewanghong@ntu.edu.sg).

Y. Zhang and Z. Niu are with the Institute of Semiconductors, Chinese Academy of Sciences, Beijing 100083, China (e-mail: zhangyu@semi.ac.cn; zcnliu@semi.ac.cn).

C. Tong is with the State Key Lab of Luminescence and Applications, Changchun Institute of Optics, Fine Mechanics and Physics, Chinese Academy of Sciences, Changchun 130033, China (e-mail: tongcz@ciomp.ac.cn).

C. Liu is with the Temasek Laboratories, Nanyang Technological University, Singapore 637553 (e-mail: liucy@ntu.edu.sg).

Color versions of one or more of the figures in this paper are available online at <http://ieeexplore.ieee.org>.

Digital Object Identifier 10.1109/JSTQE.2016.2553448

region to the underlying Si waveguide region. A tapered structure has been demonstrated to efficiently facilitate coupling the light from the InP QW region to the underlying SOI waveguide [23]–[26]. However, tapered structures have not been evaluated for the GaSb QW laser integrated onto SOI platforms yet.

Conventionally, SiO_2 has been used as bonding material in direct wafer bonding of III–V materials onto SOI waveguides [15]. But due to its large thermal resistivity ($\sim 71.43 \text{ K} \cdot \text{cm/W}$) [27], heat dissipation becomes a big problem, especially for lasers whose performances are affected significantly by thermal properties. Benzocyclobutene is also widely used in adhesive wafer bonding, but its thermal resistivity is even larger ($\sim 344.83 \text{ K} \cdot \text{cm/W}$) [28]. Recently, we have reported the low temperature heterogeneous InP bonding on a Si wafer with an Al_2O_3 bonding layer [29], [30]. Due to its much lower thermal resistivity ($\sim 2.56 \text{ K} \cdot \text{cm/W}$) [31], Al_2O_3 becomes a very promising candidate for bonding III–V lasers onto SOI wafers. With Al_2O_3 bonding layer, we have previously reported the InP-based untravelling carrier photodiode bonded onto a SOI platform with improved thermal characteristics [18].

In this paper, for the first time, we investigate a GaSb QW laser, with a tapered waveguide structure, bonded onto SOI circuits with an Al_2O_3 bonding layer. The thermal resistance has been calculated and compared to that with a SiO_2 bonding layer. The tapered-waveguide GaSb QW laser which is suitable for integration onto SOI circuits has been designed and grown with molecular beam epitaxy (MBE). The fabricated standalone GaSb QW laser worked under CW operation with emission wavelength of 2019 nm at room temperature with a low threshold current of 37 mA. With our design, simulated by a RSOFT BeamProp software [32], the light in the GaSb QW active region can be successfully coupled into the underlying SOI waveguide. In addition, the use of Al_2O_3 bonding layer potentially enhances the thermal characteristics of this device. By comparing the device's thermal property with the same structure using SiO_2 bonding layer, we show that device with Al_2O_3 bonding layer has a much lower ($\sim 70\%$) thermal resistance.

II. DEVICE STRUCTURE

The schematic diagram of the proposed device structure, i.e., a tapered-waveguide GaSb QW laser bonded onto a SOI waveguide with an Al_2O_3 bonding layer, and its cross section are shown in Fig. 1. For the entire device, the width of the Si waveguide W_{Si} is kept uniform while the width of the III–V structure varies along the Z axis (in the main light amplification region, the width of III–V structure is $4 \mu\text{m}$ as shown in Fig. 1). The length of the entire III–V region is $1000 \mu\text{m}$, including two tapered coupling structures ($50 \mu\text{m}$ each) and a $900\text{-}\mu\text{m}$ -long uniform region. Light emitted from the III–V laser can be coupled into the Si waveguide gradually through the tapered coupling structures and can keep oscillating in it. Every time passing through the III–V region, the light is coupled back into the III–V laser and gets amplified.

III. LASER RESULTS

Before simulations of the hybrid device, the GaSb-based III–V lasers, which are used for bonding onto SOI wafers, have

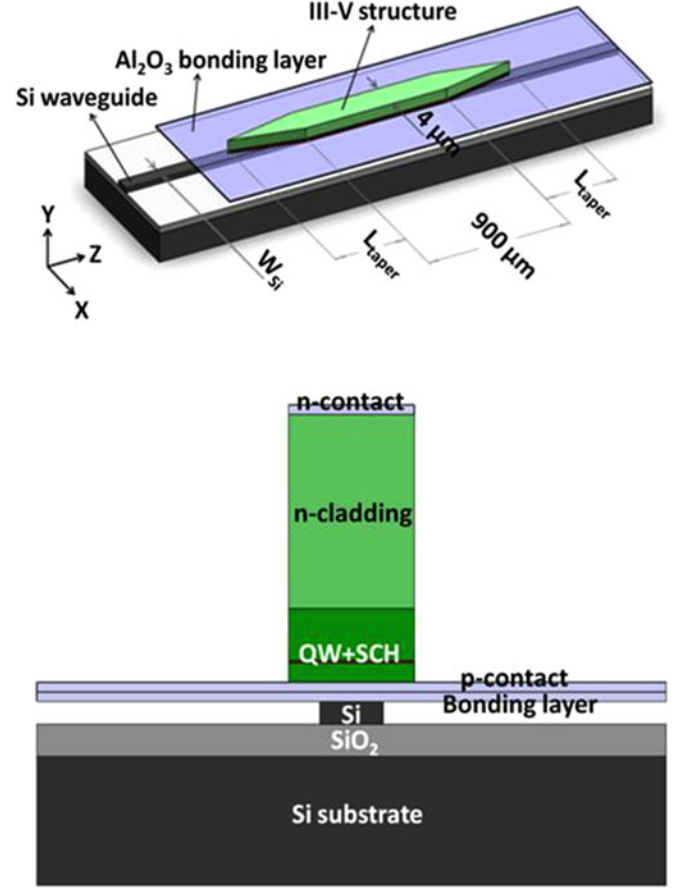


Fig. 1. Schematic diagram of the entire device and its cross section (not to scale).

TABLE I
EPITAXIAL STRUCTURE OF LASER

Layer	MATERIAL	Thickness (nm)
7	GaSb	250
6	$\text{Al}_{0.5}\text{GaAsSb}$	1500
5	$\text{Al}_{0.2}\text{GaAsSb}$	270
4	$\text{In}_{0.2}\text{Ga}_{0.8}\text{Sb}$	10
3	$\text{Al}_{0.2}\text{GaAsSb}$	270
2	$\text{Al}_{0.5}\text{GaAsSb}$	1500
1	GaSb	500
0	GaSb	$700 \mu\text{m}$

been fabricated and tested. The epitaxial structure of the laser was grown with MBE and has been shown in Table I. The detailed growth process is similar to that described in [33]. The laser structure has been calculated by 8-band k dot p method [34], same as we performed in [35]. The results are shown in Fig. 2, including the first two electron subbands and the first three heavy-hole bands. The fundamental transition is $\sim 2.0 \mu\text{m}$.

The device fabrication process is the same as we published before [36], [37]. Standard photolithography and wet chemical etching at room temperature was carried out to form the ridge. A SiO_2 layer was deposited on the wafer for injection current confinement. Ti/Au and Ni/Ge/Au/Ni/Au were evaporated on

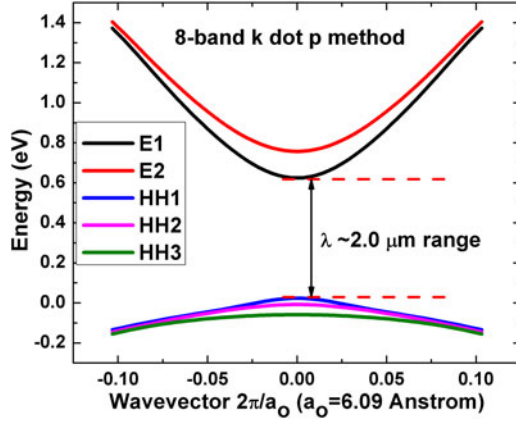


Fig. 2. $\text{In}_{0.2}\text{Ga}_{0.8}\text{Sb}/\text{Al}_{0.2}\text{GaAsSb}$ QW bandgap calculation.

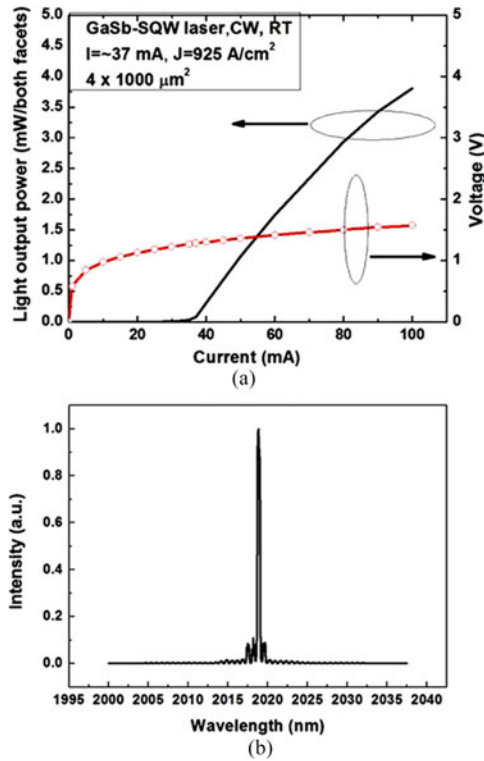


Fig. 3. (a) LIV curve and (b) lasing spectrum of the GaSb laser.

top and bottom of the GaSb laser to form ohmic contact. The light output power and voltage versus injection current (LIV) curve is shown in Fig. 3(a). The output power corresponds to both facets of the laser. As can be seen from the figure, the single QW GaSb laser works well in CW mode at room temperature with a threshold current of 37 mA. Lasing spectrum has also been measured using an optical spectrum analyzer (OSA) when the laser was driven slightly above threshold at 48 mA and shown in Fig. 3(b). The lasing spectrum peaks at around 2019 nm, which agrees well with the design in Fig. 2.

Fig. 4 shows the net modal gain ($G_{\text{net}} = \Gamma \cdot g - \alpha_i$) spectra from the fabricated GaSb laser at 20 °C at several bias currents.

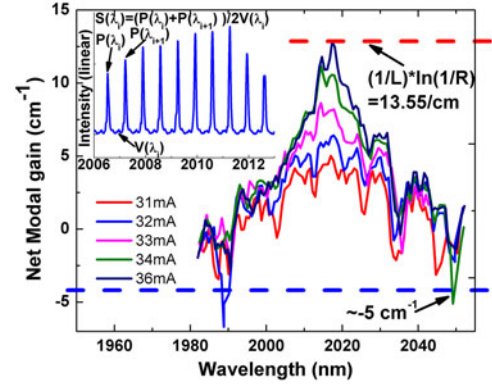


Fig. 4. Net modal gain versus injection current at room temperature from a GaSb QW laser. The inset shows the FP spectra in greater detail.

G_{net} is computed from multiple amplified spontaneous emission (ASE) spectra obtained at different injection currents using Eq. (1) [36], [38]. The ASE spectra were recorded with a high resolution OSA (AQ6375, 1200–2400 nm) with the step size of 0.01 nm and the spectral resolution of 0.01 nm. The spectral resolution in the measurement is considered very good compared to the adjacent longitudinal FP mode spacing in our presented laser, which is about 0.6 nm. This could ensure obtaining the reliable data using Eq. (1). The inset of Fig. 4 shows the FP modes in greater detail. The sharp peak and valley indicate excellent mode spacing as expected. In calculating the G_{net} , we used the known laser cavity length L_c . The laser facet reflectivity R is determined by $[(n-1)/(n+1)]^2$, where n is the group refractive index, obtained from the ASE spectrum. It can be seen from Fig. 4 that, when the current is 36 mA, just below the threshold (37 mA), the maximum gain is reached. Assuming a modal gain of zero at long wavelengths, we extract the internal loss (α_i) to be $\sim -5 \text{ cm}^{-1}$, which indicates the high quality of the designed GaSb laser structure

$$G_{\text{net}}(\lambda) = \Gamma g_{\text{material}}(\lambda) - \alpha_i = \frac{1}{L} \ln \frac{\sqrt{S(\lambda)} - 1}{\sqrt{S(\lambda)} + 1} + \frac{1}{2L} \ln \left(\frac{1}{R_1 R_2} \right) \quad (1)$$

where α_i is the internal loss, S is the ratio of intensity maximum $P(\lambda)$, and minimum $V(\lambda)$ in the consecutive FP resonances in the whole wavelength range [38], as expressed in the inset of Fig. 4, L_c is the cavity length, and R_1 and R_2 are facet reflectivities.

IV. EVANESCENT COUPLING SIMULATIONS

The entire hybrid device using the same epitaxial structure with the tested lasers (for bonding purpose, we changed the thickness of the p-side waveguide layer and removed the p-side cladding layer) has been generated with beam propagation method (BPM) by a RSOF BeamProp software. The details of the III–V structure integrated onto the SOI platform, from the Si waveguide surface to the III–V side, are 50-nm-thick bonding layer, 50-nm-thick GaSb contact layer, 100-nm-thick p-type $\text{Al}_{0.2}\text{GaAsSb}$ waveguide layer, 10-nm-thick $\text{In}_{0.2}\text{Ga}_{0.8}\text{Sb}$

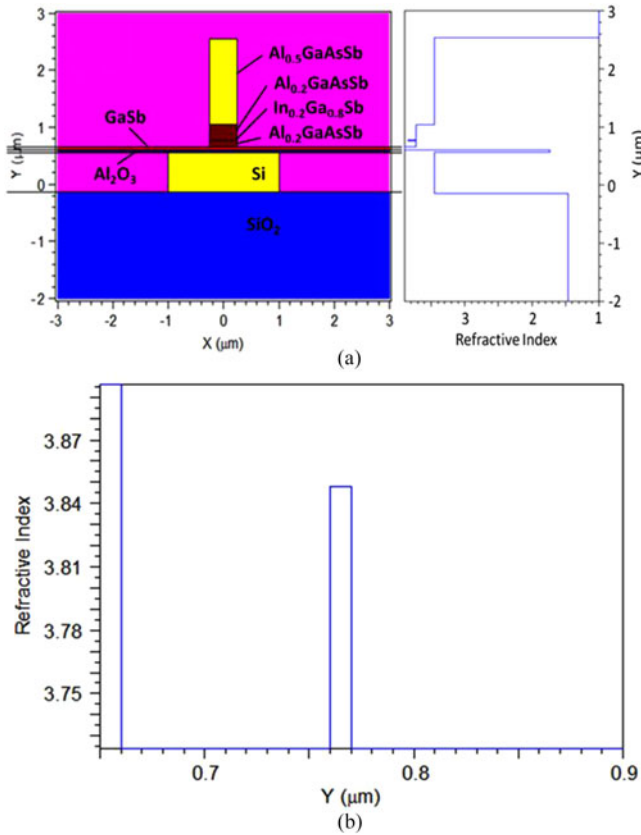


Fig. 5. (a) Refractive index profile of the entire device and (b) detailed profile of the QW.

TABLE II
EPITAXIAL STRUCTURE OF LASER

Material	Refractive Index
Si	3.451
SiO ₂	1.465
Al ₂ O ₃	1.738
GaSb	3.896
Al _{0.5} GaAsSb	3.457
Al _{0.2} GaAsSb	3.724
In _{0.2} Ga _{0.8} Sb	3.848

QW layer, 270-nm-thick n-type Al_{0.2}GaAsSb waveguide layer and 1500-nm-thick n-type Al_{0.5}GaAsSb cladding layer.

Fig. 5 shows the refractive index profile of the entire device (GaSb QW laser onto SOI waveguide) (a) as well as the enlarged refractive index profile of its In_{0.2}Ga_{0.8}Sb QW active region (b). The specific values of the refractive indices used in the BPM simulation are given in Table II [22], [39]–[42]. For the refractive index determination of the InGaSb material, we use the method described in [39]. The equations are expressed as

$$\varepsilon_1(\omega) = A \left[f(\chi_0) + \frac{1}{2} [E_0 / (E_0 + \Delta_0)]^{1.5} f(\chi_{OS}) \right] + B \quad (2)$$

$$n(\omega) = \varepsilon_1(\omega)^{0.5} \quad (3)$$

where A and B are the constant terms arising mainly from the energy bandgaps of the material, E_0 is direct bandgap energy, Δ_0 is spin orbit splitting energy, ω is circular frequency and

$$f(\chi_0) = \chi_0^{-2} \left[2 - (1 + \chi_0)^{0.5} - (1 - \chi_0)^{0.5} H(1 - \chi_0) \right] \quad (4)$$

$$f(\chi_{OS}) = \chi_{OS}^{-2} \left[2 - (1 + \chi_{OS})^{0.5} - (1 - \chi_{OS})^{0.5} H(1 - \chi_{OS}) \right] \quad (5)$$

$$\chi_0 = \hbar\omega / E_0 \quad (6)$$

$$\chi_{OS} = \hbar\omega / (E_0 + \Delta_0) \quad (7)$$

and

$$H(y) = \begin{cases} 1 & \text{for } y \geq 0 \\ 0 & \text{for } y < 0 \end{cases} \quad (8)$$

where \hbar is Planck constant divided by 2π .

For the refractive index determination of AlGaAsSb materials lattice matched with GaSb, an improved single-effective-oscillator model [40] is used and the equations are expressed as

$$n^2 - 1 = \frac{E_d}{E_0} + E^2 \frac{E_d}{E_0^3} + \frac{\eta}{\pi} E^4 \ln \left(\frac{E_f^2 - E^2}{E_\Gamma^2 - E^2} \right) \quad (9)$$

$$E_f^2 = 2E_0^2 - E_\Gamma^2 \quad (10)$$

$$\eta = \pi E_d / 2E_0^3 (E_0^2 - E_\Gamma^2) \quad (11)$$

where E is the photon energy $\hbar\nu$, E_0 and E_d are two single-effective-oscillator parameters and E_Γ is the direct bandgap energy.

In order to find proper widths of the Si waveguide and III–V structure, a series of optical mode distribution simulations using both Al₂O₃ and SiO₂ as bonding materials have been carried out. The details of the simulation procedure are as follows: the width of the Si waveguide was kept constant at 2 μm and the width of the III–V structure was varied from significantly less than 2 μm (0.3 μm) to 4 μm . The thickness of the bonding layer is 50 nm. As can be seen from the results shown in Fig. 6 (two curves with circular symbols), there is almost no difference in light power in the Si waveguide by using either Al₂O₃ or SiO₂ bonding layer. And when the III–V structure is very narrow, like less than 0.4 μm , almost all the light is coupled into the Si waveguide. Then there is a dramatic change when the width of the III–V structure exceeds 0.4 μm , which is the portion of light in the Si waveguide decreases rapidly due to the better confinement of the III–V structure. Then when the width of the III–V structure increases further to more than 0.8 μm , light distribution changes only marginally.

This is the basic idea of taper coupling and it is widely used for evanescent coupling in III–V on SOI hybrid devices [23]–[26]. Due to the width change of the III–V structure along the taper, light also redistributes. Fig. 7 shows the top view of the device together with optical mode distributions at different positions of the Z axis. At the main amplification region (a) where both

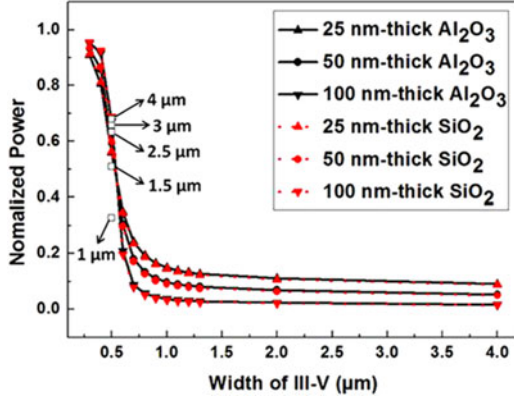


Fig. 6. Normalized power in the Si waveguide when either the III-V structure or Si waveguide width changes.

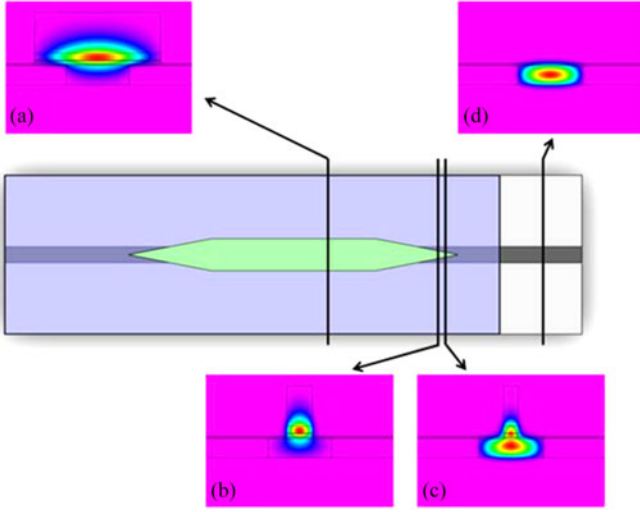


Fig. 7. Optical mode distributions at different positions of the Z axis.

width and refractive index of the III-V structure are larger than the Si waveguide, almost all the optical mode distributes in the III-V structure. In the taper coupling region (b), (c), optical mode starts to emerge in the Si waveguide and the narrower the III-V structure is, the more portions of optical mode stay in the Si waveguide. When there is no III-V structure above the Si waveguide (d), the optical mode stays in the Si waveguide only. These results confirm the relationship between optical mode distributions and structure widths shown in Fig. 6.

In addition, we can also tune the width of the Si waveguide while keeping the width of the III-V structure at a modest value, like $0.5 \mu\text{m}$. The simulation results have been shown in Fig. 6 (the discrete points) together with the corresponding Si waveguide widths. So far, the optical mode distributions can be tuned freely by adjusting the structure widths.

Besides the variation of widths, three bonding layer thicknesses (25 nm, 50 nm and 100 nm) are also used to study their influences on the coupling efficiency. As can be seen from Fig. 6, for the three thicknesses, the difference in light power in the Si waveguide by using either Al_2O_3 or SiO_2 bonding layer

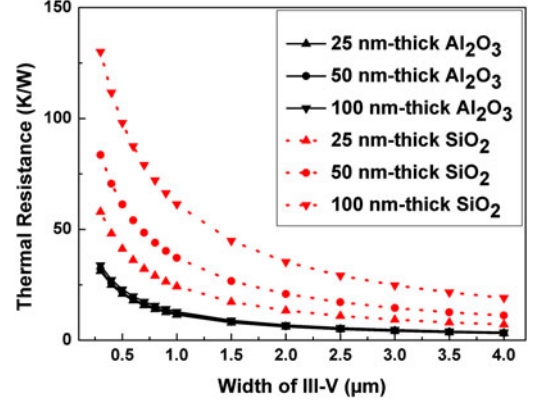


Fig. 8. Thermal resistance for downward transfer of heat flux.

is trivial, which indicates no compromise in optical coupling efficiency when Al_2O_3 is used to replace the conventional SiO_2 as bonding material. The bonding layer thickness does have some influence on the coupling efficiency. Overall, less light remains in the Si waveguide for thicker bonding layers, which could be beneficial for light amplification.

V. THERMAL RESISTANCE

Since the SOI wafer is wide enough compared to the III-V lasers, the total thermal resistance for downward transfer of heat flux can be seen as the sum of resistance of each layer from the active region of the GaSb laser where heat is generated to the Si waveguide, and it can be calculated by a constant heat spreading model [43]. The model has been widely used in hybrid devices and other electronic and photonic devices such as HBTs and lasers [44], [45].

The III-V structure was calculated as a rectangle in the X-Z plane with length L and width W . The length L was kept constant at $1000 \mu\text{m}$ while the width W was varied from $0.3 \mu\text{m}$ to $2 \mu\text{m}$ during the calculations. For bonding layer thickness, we also chose the three values used in coupling efficiency simulations to test whether it is a critical factor for total thermal resistance. The expression of thermal resistance is

$$R_\theta = \int_0^{D_i} \frac{\theta}{(L + 2x)(W + 2x)} dx \quad (12)$$

where D_i is the thickness of the calculated layers, θ is the thermal conductivity.

As can be seen from the results in Fig. 8, there are significant reductions in thermal resistance by using Al_2O_3 as the bonding material no matter how thick the bonding layer is. And bonding thickness barely affects the total thermal resistance when Al_2O_3 is used due to its low thermal resistivity. In the main light amplification region where the width of the III-V structure W equals $4 \mu\text{m}$, the thermal resistance is reduced around 70% when the thickness of the bonding layer is 50 nm.

VI. CONCLUSION

In this work, a tapered waveguide GaSb QW laser, bonded onto SOI circuits with an Al_2O_3 bonding layer is designed and analyzed. The standalone GaSb QW lasers grown by MBE to be integrated on SOI has demonstrated CW operation with emission wavelength of 2019 nm at room temperature. It shows a low threshold current of 37 mA. The BPM simulations show that, with our design, the light in the GaSb QW active region can be successfully coupled into the underlying SOI waveguide. The thermal property of the GaSb-on-Si laser has been calculated using a constant heat spreading model, and results show that the devices using Al_2O_3 bonding layer has a much lower ($\sim 70\%$) thermal resistance as compared to the one using SiO_2 bonding layer. Our results suggest that Al_2O_3 bonding layer could be a promising candidate for GaSb lasers integrated on SOI circuits, where thermal dissipation could be critical. The above-mentioned method is also useful for our future SOI integrated GaSb distributed feedback lasers, with laterally coupled Bragg grating, as well as GaSb mode-locked lasers.

ACKNOWLEDGMENT

The authors would like to thank Prof. S. S. Kathpalia for English correction.

REFERENCES

- [1] C. E. Miller and L. R. Brown, "Near infrared spectroscopy of carbon dioxide I. $^{16}\text{O}^{12}\text{C}^{16}\text{O}$ line positions," *J. Mol. Spectrosc.*, vol. 228, no. 2, pp. 329–354, Dec. 2004.
- [2] M. Buchwitz, V. V. Rozanov, and J. P. Burrows, "A near-infrared optimized DOAS method for the fast global retrieval of atmospheric CH_4 , CO , CO_2 , H_2O , and N_2O total column amounts from SCIAMACHY Envisat-1 nadir radiances," *J. Geophys. Res.*, vol. 105, no. D12, pp. 15231–15245, Jun. 2000.
- [3] D. J. Richardson, "Filling the light pipe," *Science*, vol. 330, no. 6002, pp. 327–328, Oct. 2010.
- [4] J. J. Ackert *et al.*, "High-speed detection at two micrometres with monolithic silicon photodiodes," *Nature Photon.*, vol. 9, no. 6, pp. 393–396, 2015.
- [5] G. Roelkens *et al.*, "Silicon-based photonic integration beyond the telecommunication wavelength range," *IEEE J. Sel. Topics Quantum Electron.*, vol. 20, no. 4, pp. 394–404, Jul./Aug. 2014.
- [6] W. Lei and C. Jagadish, "Lasers and photodetectors for mid-infrared 2–3 μm applications," *J. Appl. Phys.*, vol. 104, pp. 091101-1–091101-11, 2008.
- [7] S. Luo *et al.*, "High performance 2150 nm-emitting InAs/InGaAs/InP quantum well lasers grown by metalorganic vapor phase epitaxy," *Opt. Exp.*, vol. 23, no. 7, pp. 8383–8388, Apr. 2015.
- [8] G. Turner, H. Choi, and M. Manfra, "Ultralow-threshold (50 A/cm 2) strained single-quantum-well GaInSb/AlGaAsSb lasers emitting at 2.05 μm ," *Appl. Phys. Lett.*, vol. 72, no. 8, pp. 876–878, Feb. 1998.
- [9] L. Shterengas, G. Belenky, M. Kisin, and D. Donetsky, "High power 2.4 μm heavily strained type-I quantum well GaSb-based diode lasers with more than 1 W of continuous wave output power and a maximum power-conversion efficiency of 17.5%," *Appl. Phys. Lett.*, vol. 90, no. 1, pp. 011119-1–011119-3, Jan. 2007.
- [10] S. K. Selvaraja, W. Bogaerts, P. Dumon, D. Van Thourhout, and R. Baets, "Subnanometer linewidth uniformity in silicon nanophotonic waveguide devices using CMOS fabrication technology," *IEEE J. Sel. Topics Quantum Electron.*, vol. 16, no. 1, pp. 316–324, Jan./Feb. 2010.
- [11] G. T. Reed, "Device physics: The optical age of silicon," *Nature*, vol. 427, no. 6975, pp. 595–596, Feb. 2004.
- [12] A. W. Fang *et al.*, "Electrically pumped hybrid AlGaInAs-silicon evanescent laser," *Opt. Exp.*, vol. 14, no. 20, pp. 9203–9210, Oct. 2006.
- [13] H. Park, A. Fang, S. Kodama, and J. Bowers, "Hybrid silicon evanescent laser fabricated with a silicon waveguide and III-V offset quantum wells," *Opt. Exp.*, vol. 13, no. 23, pp. 9460–9464, Nov. 2005.
- [14] X. Sun and A. Yariv, "Engineering supermode silicon/III-V hybrid waveguides for laser oscillation," *J. Opt. Soc. Amer. B*, vol. 25, no. 6, pp. 923–926, Jun. 2008.
- [15] X. Luo *et al.*, "High-throughput multiple dies-to-wafer bonding technology and III/V-on-Si hybrid lasers for heterogeneous integration of optoelectronic integrated circuits," *Frontier Mater.*, vol. 2, Apr. 2015, Art. no. 28.
- [16] G. Roelkens, D. Van Thourhout, R. Baets, and M. Smit, "Laser emission and photodetection in an InP/InGaAsP layer integrated on and coupled to a Silicon-on-Insulator waveguide circuit," *Opt. Exp.*, vol. 14, no. 18, pp. 8154–8159, Sep. 2006.
- [17] N. Hattasan *et al.*, "GaSb-based integrated lasers and photodetectors on a Silicon-On-Insulator waveguide circuit for sensing applications in the shortwave infrared," in *Proc. Photon. Global Conf.*, Dec. 2012, pp. 1–4.
- [18] B. Gao *et al.*, "Design and analysis of InP-based waveguide unidirectional carrier photodiode integrated on Silicon-on-Insulator through Al_2O_3 bonding layer," *IEEE Photon. J.*, vol. 6, no. 5, Oct. 2014, Art. no. 1–6.
- [19] Y. L. Cao *et al.*, "Hybrid III-V/silicon laser with laterally coupled Bragg grating," *Opt. Exp.*, vol. 23, no. 7, pp. 8800–8808, Apr. 2015.
- [20] X. N. Hu *et al.*, "Relative intensity noise of silicon hybrid laser," *IEEE J. Quantum Electron.*, vol. 50, no. 6, pp. 466–473, Jun. 2014.
- [21] R. Ferrini, M. Patrini, and S. Franchi, "Optical functions from 0.02 to 6 eV of $\text{Al}_x\text{Ga}_{1-x}\text{Sb}$ /GaSb epitaxial layers," *J. Appl. Phys.*, vol. 84, no. 8, pp. 4517–4524, Oct. 1998.
- [22] H. H. Li, "Refractive index of silicon and germanium and its wavelength and temperature derivatives," *J. Phys. Chem. Reference Data*, vol. 9, no. 3, pp. 561–658, Jul. 1980.
- [23] A. W. Fang *et al.*, "A distributed Bragg reflector silicon evanescent laser," *IEEE Photon. Technol. Lett.*, vol. 20, no. 20, pp. 1667–1669, Oct. 2008.
- [24] S. Keyvaninia *et al.*, "Demonstration of a heterogeneously integrated III-V/SOI single wavelength tunable laser," *Opt. Exp.*, vol. 21, no. 3, pp. 3784–3792, Feb. 2013.
- [25] M. Lamponi *et al.*, "Low-threshold heterogeneously integrated InP/SOI lasers with a double adiabatic taper coupler," *IEEE Photon. Technol. Lett.*, vol. 24, no. 1, pp. 76–78, Jan. 2012.
- [26] B. Ben Bakir *et al.*, "Electrically driven hybrid Si/III-V Fabry-Pérot lasers based on adiabatic mode transformers," *Opt. Exp.*, vol. 19, no. 11, pp. 10317–10325, May. 2011.
- [27] W. M. Haynes, *CRC Handbook of Chemistry and Physics*. 95th ed. New York, NY, USA: CRC Press, 2014.
- [28] G. Roelkens *et al.*, "III-V/silicon photonics for on-chip and intra-chip optical interconnects," *Laser Photon. Rev.*, vol. 4, no. 6, pp. 751–779, Nov. 2010.
- [29] J. Fan *et al.*, "Thermal characteristics of InP- Al_2O_3 /Si low temperature heterogeneous direct bonding for photonic device integration," *ECS J. Solid State Sci. Technol.*, vol. 2, no. 9, pp. N169–N174, Jun. 2013.
- [30] P. Anantha and C. Tan, "Homogeneous chip to wafer bonding of InP- Al_2O_3 -Si using UV/ O_3 activation," *ECS J. Solid State Sci. Technol.*, vol. 3, no. 4, pp. P43–P47, Jan. 2014.
- [31] G. Becker, C. Lee, and Z. Lin, "Thermal conductivity in advanced chips: Emerging generation of thermal greases offers advantages," *Adv. Packag.*, vol. 14, no. 7, pp. 14–17, Feb. 2005.
- [32] BeamPROP. (2012). [Online]. Available: <http://optics.synopsys.com/>
- [33] Y. Zhang *et al.*, "MBE growth and fabrication of 2.4 μm InGaAsSb/AlGaAsSb laser," *Proc. SPIE*, vol. 9267, pp. 926710-1–926710-7, 2014.
- [34] S. L. Chuang, *Physics of Optoelectronic Devices*. New York, NY, USA: Wiley, 1995.
- [35] S. T. Ng *et al.*, "Investigation of the optical properties of InGaAsN/GaAs/GaAsP multiple-quantum-well laser with 8-band and 10-band k dot p model," *J. Appl. Phys.*, vol. 96, no. 8, pp. 4663–4665, Oct. 2004.
- [36] C. Liu, H. Wang, Q. Meng, B. Gao, and K. S. Ang, "Modal gain and photoluminescence investigation of two-state lasing in GaAs-Based 1.3 μm InAs/InGaAs quantum dot lasers," *Appl. Phys. Exp.*, vol. 6, no. 10, pp. 102702-1–102702-4, Oct. 2013.
- [37] C. Liu *et al.*, "Fabrication of high-performance InGaAsN ridge waveguide lasers with pulsed anodic oxidation," *IEEE Photonics Technol. Lett.*, vol. 16, no. 11, pp. 2409–2411, Nov. 2004.
- [38] B. W. Hakki and T. L. Paoli, "Gain spectra in GaAs double heterostructure injection lasers," *J. Appl. Phys.*, vol. 46, no. 3, pp. 1299–1306, Mar. 1975.

- [39] S. Adachi, "Band gaps and refractive indices of AlGaAsSb, GaInAsSb, and InPAsSb: Key properties for a variety of the 2–4 μm optoelectronic device applications," *J. Appl. Phys.*, vol. 61, no. 10, pp. 4869–4876, May 1987.
- [40] C. Alibert, M. Skouri, A. Joullie, M. Benouna, and S. Sadiq, "Refractive indices of AlSb and GaSb-lattice-matched $\text{Al}_x\text{Ga}_{1-x}\text{As}_y\text{Sb}_{1-y}$ in the transparent wavelength region," *J. Appl. Phys.*, vol. 69, no. 5, pp. 3208–3211, Mar. 1991.
- [41] L. Gao, F. Lemarchand, and M. Lequime, "Exploitation of multiple incidences spectrometric measurements for thin film reverse engineering," *Opt. Exp.*, vol. 20, no. 14, pp. 15734–15751, Jul. 2012.
- [42] I. Malitson and M. Dodge, "Refractive index and birefringence of synthetic sapphire," *J. Opt. Soc. Amer.*, vol. 62, no. 11, 1972, Art. no. 1405.
- [43] J. J. Licari and L. R. Enlow, *Hybrid Microcircuit Technology Handbook*, 2nd ed. Park Ridge, NJ, USA: Noyes, 1998.
- [44] H. Yang, H. Wang, K. Radhakrishnan, and C. L. Tan, "Thermal resistance of the reduced thermal conductivity in InGaAs/GaAs quantum dot lasers from chirp characteristics," *IEEE Trans. Electron. Devices*, vol. 51, no. 8, pp. 1221–1227, Aug. 2004.
- [45] H. Tan, K. K. Kamath, Z. Mi, P. Bhattacharya, and D. Klotzkin, "Analysis of the reduced thermal conductivity in InGaAs/GaAs quantum dot lasers from chirp characteristics," *Appl. Phys. Lett.*, vol. 89, no. 12, pp. 121116-1–121116-3, Sep. 2006.



Xiang Li received the B.Sc. and M.Sc. degrees from the Harbin Institute of Technology, Harbin, China, in 2011 and 2013, respectively. He is currently working toward the Ph.D. degree at the School of Electrical and Electronic Engineering, Nanyang Technological University, Singapore. He joined Nanyang Technological University in 2015. He is currently working on research of semiconductor lasers.



Hong Wang received the B.Eng. degree from Zhejiang University, Hangzhou, China, in 1988, and the M.Eng. and Ph.D. degrees from the Nanyang Technological University, Singapore, in 1998 and 2001, respectively. From 1988 to 1994, he was with the Institute of Semiconductors, Chinese Academy of Sciences, Beijing, China. From 1994 to 1995, he was a Royal Research Fellow with British Telecommunications Laboratories, Ipswich, U.K., where he was involved with the development of InP-based heterostructure field-effect transistors using E-beam

lithography. Since 1996, he has been with Nanyang Technological University, where he is currently an Associate Professor, and the Director of Nanyang NanoFabrication Centre. He has authored or coauthored more than 230 technical papers. He received the 2007 Defence Technology Prize, Ministry of Defence, Singapore. He served as the Session Chair, and a Subcommittee Member for 2009 and 2010 IEDM.

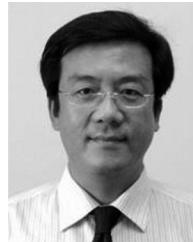


Zhongliang Qiao received the Ph.D. degree in engineering optics from the National Key Laboratory on High Power Semiconductor Lasers, Changchun University of Science and Technology, Jilin, China, in 2011. He was a Research Fellow in Singapore project (2011–2013) and a Postdoctoral Research Fellow (2015–present) in the School of Electrical and Electronic Engineering, Nanyang Technological University, Singapore. His current research interests include growth, design, simulation, fabrication, characterization, and analysis of high performance semiconductor

light sources, monolithically integrated multi-wavelength semiconductor laser. He has authored and coauthored more than 30 technical papers in these fields so far.



Yu Zhang received the Ph.D. degree in microelectronics and solid electronics from the Institute of Semiconductors, Chinese Academy of Sciences, Beijing, China. He became a Research Associate in 2015. His research interests include MBE growth and fabrication of antimonide mid-infrared high power laser, narrow-line width lasers and short-pulse lasers.



Zhichuan Niu received the Doctorate degree in physics from Institute of Semiconductors, Chinese Academy of Sciences, Beijing, China, in 1996. He is currently a Professor of the State Key Laboratory of Superlattices and Microstructures, Institute of Semiconductors, Chinese Academy of Sciences, Beijing. He is also a Collaboration Professor of the Synergetic Innovation Center of Quantum Information and Quantum Physics, University of Science and Technology of China, Hefei, China. From 1996 to 1998, he was a Postdoctoral Fellow in Paul Drude Institute

for Solid State Electronics, Berlin, Germany. From later 1998 to 1999, he worked as a Research Assistant in the University of Southern California, Los Angeles, CA, USA. He was Awarded by Hundred Talent Program of Chinese Academy of Sciences in 1999 and the Winner of the National Outstanding Youth Fund in 2006. His current works focused on MBE growth of InAs quantum dot single photon source devices, InGaAsSb long wavelength quantum well lasers, and InAs/GaSb superlattice detectors.



Cunzhu Tong (M'09) received the B.S. and M.S. degrees in physics from Chongqing University, Chongqing, China, the Ph.D. degree from the Institute of Semiconductors, Chinese Academy of Sciences (CAS), Beijing, China. He was a Research Fellow with Nanyang Technological University, Singapore from 2005 to 2009. After that, he joined the Edward S. Rogers Sr. Department of Electrical and Computer Engineering, University of Toronto, Toronto, ON, Canada, as a Postdoctoral Researcher. He became the Professor of Hundred Talents Program in

CAS and was with the Changchun Institute of Optics, Fine Mechanics and Physics, CAS, Changchun, China, in November 2010. He is the Standing Committee Member of Chinese Society of Astronautics, and received several awards including the Outstanding Young Scientist Award, Person of the Year 2012 selected by Scientific Chinese, Excellent Award of Hundred Talents Program in CAS, etc. He has authored and coauthored more than 80 refereed journal papers. His research on the low divergence diode lasers was selected as the important achievement of China optics in 2015. His current research interests include photonic crystal lasers, disk lasers, beam shaping and combining of semiconductor lasers.



Chongyang Liu (M'07) received the Ph.D. degree in semiconductor photonics from Nanyang Technological University (NTU), Singapore, in 2004. He is currently the Principal Investigator/Senior Research Scientist at Temasek Laboratories, NTU. He was a Research Associate in Singapore-MIT Alliance project (2004–2005) and a Postdoctoral Research Fellow (2005–2007) in the School of Electrical and Electronic Engineering, NTU, Singapore. From 2007 to 2009, he was a Senior Research Fellow with the A*STAR "VIP" program on Nanophotonics and Nano

electronic Integration at Data Storage Institute, Singapore. From October 2009 to January 2012, he received Humboldt Fellowship (for experienced researcher) from Alexander von Humboldt Foundation for doing research in Technical University Berlin, Germany. His research interests include design, simulation, fabrication, characterization, and analysis of low-dimensional semiconductor light sources, monolithically integrated high-speed photonic devices as well as micro/nanophotonic and electronic photonic integration. He has authored and coauthored more than 80 technical papers in these fields so far.